Computational insights on the adsorption of glycine, methionine, tyrosine and phenylalanine on the zinc oxide nanocluster $Zn_{12}O_{12}$

Seyfeddine Rahali[1] · Maamar Damous[2,3] · Youghourta Belhocine[2] · Najoua Sbei[4] · Ridha Ben Said[1] · Moussa Diawara[5] · Mahamadou Seydou[5,6]

Abstract

The current work investigated the interaction of ZnO nanoparticles (NPs) with glycine, tyrosine, methionine and phenylalanine. $(ZnO)_{12}$ cage-like cluster was modeled using the density functional theory to determine the adsorption energy, the preferred sites for adsorption of amino acids, and the electronic structure of the formed complexes. The findings suggest that pure amino acids interact with $(ZnO)_{12}$ via a chemisorption process. The thermodynamic parameters computed showed that the complexation is an exothermic process and enthalpy-driven. The oxygen atoms in the carboxyl groups of the four studied amino acids are involved in the adsorption process. PHE_$Zn_{12}O_{12}$ exhibits the highest adsorption energy (− 207.50 kJ/mol) due to its interaction with the $Zn_{12}O_{12}$ nanocluster through two different adsorption sites. The electronic and sensing properties were examined by analyzing the HOMO and LUMO energies and the HOMO–LUMO energy gap (|ΔEg|). The sensitivity of $Zn_{12}O_{12}$ nanocluster toward the studied amino acids was examined by comparing the percentage variation of the gap after the adsorption, which can reach the value of 38%, suggesting the potential of $Zn_{12}O_{12}$ nanocluster as a promising sensor for the detection of amino acids. Interaction region indicator (IRI) analysis was performed for a visual understanding of the different interactions occurring between the amino acids and the $Zn_{12}O_{12}$ nanocluster. The results of this study can shed some light on the possible application of ZnO-based nanobiosensors for detecting protein tyrosine/tryptophan nitration as an early symptom of several serious chronic diseases.

Keywords Zinc oxide · Amino acids · Density functional theory · Nanobiosensors

✉ Seyfeddine Rahali
saif.rahali@gmail.com

[1] Department of Chemistry, College of Science and Arts At Ar-Rass, Qassim University, Buraydah, Saudi Arabia

[2] Laboratory of Catalysis, Bioprocess and Environment, Department of Process Engineering, Faculty of Technology, 20 August 1955 University of Skikda, El Hadaik Road, P.O. Box 26, 21000 Skikda, Algeria

[3] Unité de Recherche de Chimie de l'Environnement et Moléculaire Structurale (URCHEMS), Département de Chimie, Université Frères Mentouri de Constantine, 25000 Constantine, Algeria

[4] Institute of Nanotechnology, Karlsruhe Institute of Technology, Eggenstein Leopoldshafen, 76344 Karlsruhe, Germany

[5] Laboratoire de Centre de Calcul de Modélisation Et de Simulation (CCMS), DER de Physique de La Faculté des Sciences et Techniques (FST), Université des Sciences des Techniques et des Technologies de Bamako (USTTB-Mali), Bamako, Mali

[6] Université Paris Cité. CNRS, ITODYS, 75013 Paris, France

1 Introduction

Nanotechnology has served as a platform for the development of innovative devices and processes for a wide variety of applications [1–3], ranging from high-tech electronics and communication to the intricate and sensitive realm of forensic inquiry. In this respect, medicine was without a doubt one of the first scientific disciplines to utilize nanodevices and nanomaterials in order to improve illness prevention, diagnostic, and treatment approaches [4, 5]. Nanostructured materials have attracted a great deal of attention due to the unique features they possess and the intriguing uses that can be found for them in a wide variety of innovative new products [6, 7]. They have been placed into the categories of rods, shells, dots, sheets, and composites [8–10], depending on the overarching shape they take. While nanoparticles have already revolutionized industries like paint and solar cells, their full potential in medicine, bio-imaging [11, 12], biomarkers [13, 14], biosensing [15–17], drug delivery [18,

19] and various nano-based-targeted therapies [20, 21]) applications have been realized.

Nanoscale zinc oxide ZnO is a semiconducting metal oxide that has great potential for use in the medical field due to the high excitation binding energy that it possesses [22]. Because ZnO nanoparticles are biocompatible and exhibit bioactivity [23], they have the potential to be an interesting option for use in biological applications. Making use of this versatile compound's electrochemical activity, luminescence, and piezoelectricity can result in the production of biosensors [24]. ZnO has potential for use in theranostic systems due to the fact that it eliminates microorganisms and reduces the risk of cancer [25, 26].

- Various $(ZnO)_n$ nanostructures, such as nanoclusters, nanohorns, nanotubes, and nanowires, have been the subject of medical research [27]. Meanwhile, the zinc oxide-like cages $(ZnO)_{12}$ have been explored conceptually and empirically [28, 29]. $(ZnO)_{12}$ nanoclusters have been explored as potential biosensors for amino acids due to their advantageous morphological, microstructural, and electrical properties [30–32]. Amino acids are zwitterionic compounds that can be employed as promising components of devices for clinical use [33–36]. Amino acids, which are smaller building blocks, are used to assemble proteins, and the interactions between amino acids and the zinc oxide could be of use in the development of new bioconjugates. Glycine is the smallest and simplest amino acid, simultaneously exhibits both carboxylate/carboxylic and amine/ammonium moieties and thus represents a good reference object for other more complex biological molecules [37, 38]. Glycine, which has the chemical formula NH_2CH_2COOH, is the tiniest and most straightforward of all the naturally occurring amino acids. As a side chain, it merely contains a single hydrogen atom. As a direct result, glycine is capable of adopting conformations that are normally disallowed in the case of other amino acids and can offer a high level of local flexibility to both polypeptides and proteins. In the literature, A number of studies can be found in the published research that demonstrate how glycine reacts with oxide metals. Indeed, P. Chaudhuri and colleagues looked at the adsorption of glycine molecules on single-walled zigzag and armchair boron-nitrogen nanotubes. Because the hydroxyl group of the glycine binds with the SBNNT surface, this configuration is the one with the highest degree of stability [39]. In the same way, S. Irrera et al. performed an exhaustive study of glycine adsorption on the Zn–ZnO surface, from the limit of the isolated molecule to the full layer and bilayer glycine formation at the surface [40]. They found that the adsorption through both functions (carboxylate and amine) is more favorable than the adsorption through one function only [40]. Other amino acid molecules, such as tyrosine, methionine and phenylalanine, have been studied in complexation with metal oxide [41–43].

To the best of our knowledge, no attempt has been made as of yet to investigate the way in which these four amino acids interact with the zinc oxide-like cages $(ZnO)_{12}$.

It is essential to use computational molecular modeling as a tool for elaborating the mechanisms of molecular recognition between host–guest compounds [24–47]. This type of knowledge can be essential to the comprehension and development of new medicinal products for the treatment of a variety of disorders [48, 49]. The vast majority of ab initio investigations of amino acid adsorption were carried out without the presence of any solvent; hence, these studies are relevant to adsorption that occurs in the gas phase. On ZnO, the preferred pathways for amino acid adsorption are ones that require coordination, also known as the creation of covalent bonds.

Evidently, gaining an understanding of the nature of the interactions that biomolecules have with the zinc oxide-like cages $(ZnO)_{12}$ on an atomic level would provide extremely useful information for the design and manufacture of nanodevices that are meant to be employed for biomedical reasons.

In this context, the current research is aimed to investigate the binding properties between $Zn_{12}O_{12}$ nanocluster and four amino acids, namely, glycine (GLY), tyrosine (TYR), methionine (MET) and phenylalanine (PHE). Structural, energetic and electronic properties of the aminoacids_$Zn_{12}O_{12}$ complexes were determined.

2 Computational details

In computational investigations of bio-conjugated systems, the most essential thing is to discover the proper simulation units that are huge enough to match the behavior of the real sample but tiny enough to keep the cost of computing down. In other words, finding the right simulation units that are big enough to match the behavior of the real sample but small enough to keep the cost of computing down. In relation to these aspects, rather than working with a massive system containing tens of thousands of atoms, the $(ZnO)_{12}$ cluster, which contains only 24 atoms, was selected to mimic zinc oxide nanoparticles [50]. This was due to the fact that it was the most stable cage and symmetrical small ZnO cluster. The structures of $Zn_{12}O_{12}$ nanocluster and the amino acids methionine, glycine, tyrosine and phenylalanine, as well as the complexes of amino acid_$Zn_{12}O_{12}$ were fully optimized by ORCA program (version 5.0.0) [51–53] using the B3LYP functional [54, 55] associated

with def2-TZVP basis set [56] and D4 atomic-charge dependent London dispersion correction model [57], the use of the recently developed D4 dispersion correction scheme is important to improve the accurate description of chemical systems. The resolution of the identity approximation (RIJCOSX) [58] was employed to speed up the DFT calculations. A geometrical counterpoise-type correction scheme (GCP) [59] was utilized to account for the basis set superposition error (BSSE). All geometry optimization calculations were carried out using default SCF convergence criteria in ORCA program. All real 3N-6 vibrational frequencies are obtained for the optimized geometries using B3LYP-D4/ def2-TZVP level to ensure that the obtained structures have no imaginary frequencies. The adsorption energies were calculated for the most stable configurations as follows:

$$E_{ads} = E_{(\text{amino acid\_Zn12O12})} - \left(E_{Zn12O12} + E_{\text{amino acid}}\right) \quad (1)$$

where $E_{(\text{amino acid\_Zn12O12})}$ represents the adsorption energy for each amino acid on the $Zn_{12}O_{12}$ nanocluster; $E_{Zn12O12}$ and $E_{\text{amino acid}}$ represent the energies of $Zn_{12}O_{12}$ nanocluster and free amino acids, respectively. Negative values of adsorption energy correspond to an exothermic process, indicating that the formed complexes are stable, while positive values of adsorption energy indicate an unfavorable process. All the studied systems were verified as minima on the potential energy surface through frequency calculations.

3 Results and discussion

3.1 Geometric parameters of $Zn_{12}O_{12}$ nanocage

The molecular structure of $Zn_{12}O_{12}$ nanocage represented in Fig. 1 may be described as constructed from eight hexagon rings (Zn_3O_3) and six tetragon rings (Zn_2O_2), which are connected by sharing all their Zn and O atoms. The Zn–O bond lengths values range from 1.867 to 1.963 Å and are in accord with those reported in the literature [60, 61].

The shortest Zn–O distances ranging from 1.868 to 1.869 Å are observed for three alternating Zn–O bonds in the hexagons, while the longest ones in the interval (1.959–1.963 Å) correspond to all Zn–O bonds in the tetragons and the remaining three alternating Zn–O bonds in the hexagons shared with the tetragons. The bonds angles of the Zn–O-Zn and O–Zn–O in the tetragons are in the range of 87.32–91.08°, whereas those of the hexagons range from 110.73 to 127.99° with the O–Zn–O bond angles being wider than 127°. Selected bond lengths and bond angles calculated at B3LYP-D4/def2-TZVP-gCP level for $Zn_{12}O_{12}$ nanocluster are listed in Table 1.

3.2 Adsorption energies

The initial geometries with different adsorption orientations for the interaction of amino acids with the $Zn_{12}O_{12}$ nanocluster considered in this work are shown in Supplementary Data (Figure S1). The most stable complexes for each amino acid

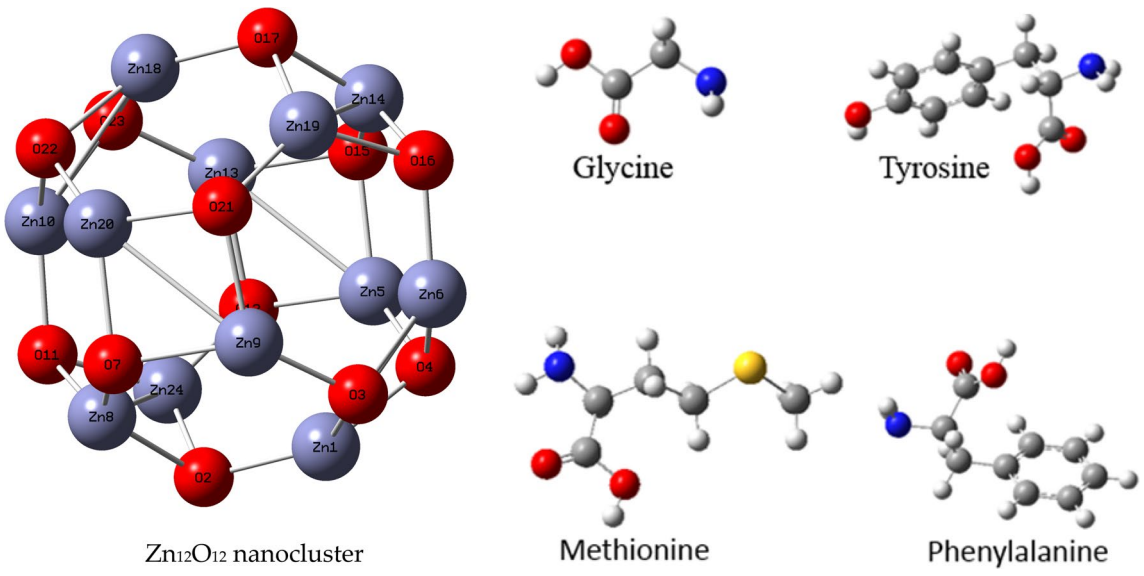

Fig. 1 Molecular structure of optimized $Zn_{12}O_{12}$ nanocluster, glycine, tyrosine, methionine and phenylalanine. Atomic color code: carbon (gray), hydrogen (white), oxygen (red), blue (nitrogen), sulfur (yellow), zinc (Corsican purple)

Table 1 Selected bond lengths (Å) and angles (°) for $Zn_{12}O_{12}$ nanocluster

Bond length (Å)		Bond angle (°)	
Zn1-O2	1.869	Zn9-O7-Zn20	87.32
Zn1-O3	1.960	Zn1-O4-Zn6	87.49
Zn1-O4	1.961	O4-Zn1-O3	90.97
Zn6-O3	1.963	O2-Zn8-O11	91.00
Zn6-O4	1.959	O16-Zn19-O17	91.08
Zn6-O16	1.868	O7-Zn20-O21	91.11
Zn9-O3	1.868	Zn1-O2-Zn8	110.73
Zn9-O7	1.962	Zn19-O21-Zn20	111.05
Zn9-O21	1.961	Zn8-O7-Zn9	111.23
Zn19-O16	1.963	O22-Zn18-O17	127.47
Zn19-O17	1.959	O12-Zn24-O11	127.75
Zn18-O17	1.869	O2-Zn1-O3	127.99

adsorbed on the $Zn_{12}O_{12}$ nanocluster are depicted in Fig. 2 using Gaussview 5.0 program [62].

The adsorption energy values (E_{ads}) of GLY_$Zn_{12}O_{12}$, TYR_$Zn_{12}O_{12}$, MET_$Zn_{12}O_{12}$ and PHE_$Zn_{12}O_{12}$ complexes calculated in vacuum at B3LYP-D4/def2-TZVP-gCP level of theory are respectively, – 147.83, – 207.50, – 161.72 and – 193.51 kJ/mol. The complexes TYR_$Zn_{12}O_{12}$ and PHE_$Zn_{12}O_{12}$ exhibit the highest adsorption energies due to their interaction with the $Zn_{12}O_{12}$ nanocluster through two different adsorption sites, as shown in Fig. 2.

The adsorption process involves the oxygen atoms of the carboxyl groups of all the amino acids. Indeed, the relaxed geometries showed that carbonyl moiety of the carboxyl groups of glycine, tyrosine, methionine and phenylalanine move toward the Zn atoms of $Zn_{12}O_{12}$ with which they establish short Zn–O bonds (1.944–1.956 Å), thus leading to the chemisorption of the amino acids on $Zn_{12}O_{12}$ nanocluster. The carboxyl groups are found more favorable to interact with the Zn atoms of the $Zn_{12}O_{12}$ nanocluster than the amino groups. In addition, tyrosine and phenylalanine are also bound to the adsorbent through the oxygen atom of the hydroxyl group of tyrosine and a carbon atom from the benzene ring of phenylalanine.

3.3 Thermodynamic analysis

Thermodynamic parameters such as the changes of Gibbs energy, enthalpy and entropy were calculated at 298.15 K and 1 atm using B3LYP-D4/def2-TZVP-gCP level of theory in a vacuum. The zero-point energy (ZPE) correction was applied in the energy calculations. The values of Gibbs free energy, enthalpy and entropy changes of the adsorption process of the amino acids on $Zn_{12}O_{12}$ nanocluster were computed at standard temperature and pressure values (298.15 K

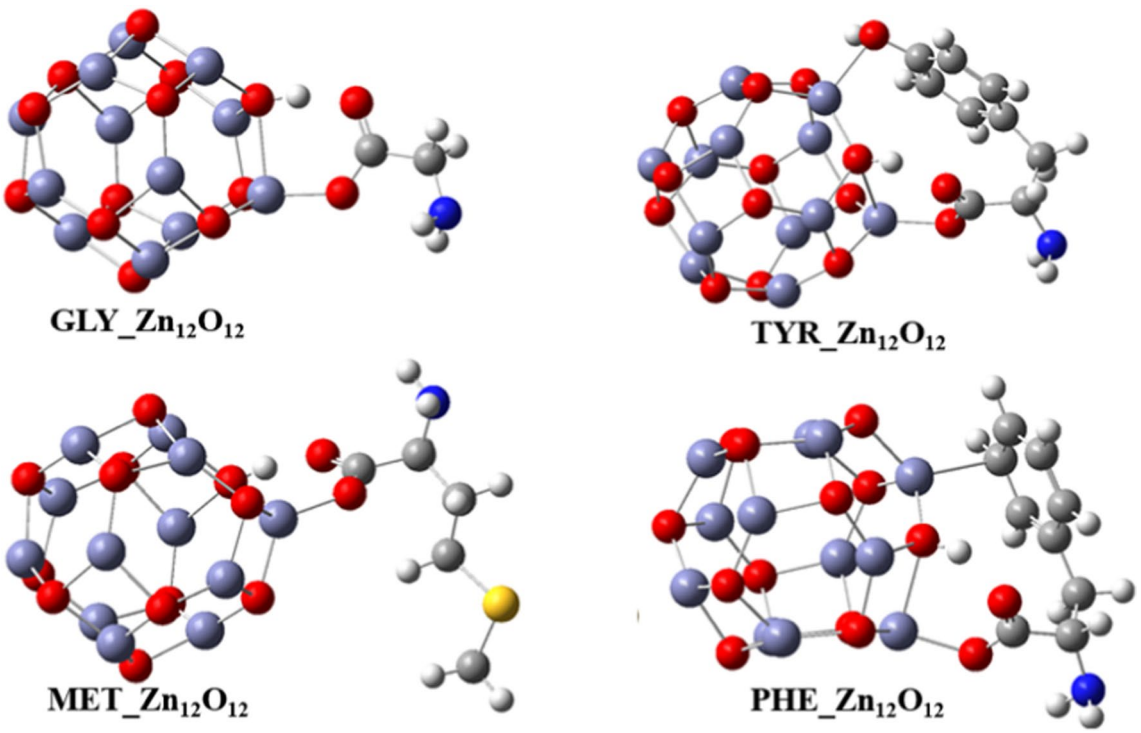

Fig. 2 Full optimized geometries in vacuum of amino acids glycine, tyrosine, methionine and phenylalanine adsorbed on $Zn_{12}O_{12}$ nanocluster. Atomic color code: carbon (gray), hydrogen (white), oxygen (red), blue (nitrogen), sulfur (yellow), zinc (Corsican purple)

and 1 atm) and listed in Table 2. Negative Gibbs energy changes for all complexes ($\Delta G < 0$), indicating that the reaction process proceeds spontaneously. The Gibbs energy of TYR_$Zn_{12}O_{12}$ and PHE_$Zn_{12}O_{12}$ are.

more negative than that of GLY_$Zn_{12}O_{12}$ and MET_$Zn_{12}O_{12}$. Moreover, the computed values of energy changes of enthalpy and entropy are also negative, showing that the complexation is an exothermic process and enthalpy-driven.

3.4 Electronic properties

The electronic properties such as the HOMO, LUMO, HOMO–LUMO gap and the percentage variation of the HOMO–LUMO gap of $Zn_{12}O_{12}$ nanocluster and the formed complexes are summarized in Table 3. As can be seen from Table 3, the HOMO energy values of the complexes are above (less negative) that of the pristine $Zn_{12}O_{12}$; the HOMO of MET_$Zn_{12}O_{12}$ has increased considerably. However, the LUMO levels were similar to the pristine $Zn_{12}O_{12}$ once the complexes were formed. The HOMO–LUMO gap value of $Zn_{12}O_{12}$ calculated at B3LYP-D4/def2-TZVP-gCP level of theory (4.25 eV) is consistent with the value reported in similar studies [28, 63, 64]. The ΔEg of the complexes is significantly reduced in comparison to that of pristine $Zn_{12}O_{12}$ and follows the decreasing order: ΔEg (PHE_$Zn_{12}O_{12}$) > ΔEg (TYR_$Zn_{12}O_{12}$) > ΔEg (GLY_$Zn_{12}O_{12}$) > ΔEg (MET_$Zn_{12}O_{12}$). By comparing the percentage change in the gap following the adsorption, we were able to investigate the degree to which the $Zn_{12}O_{12}$ nanocluster reacts to the amino acids that were under investigation. From Table 3, the percentage variation of Eg during the adsorption of glycine, tyrosine, methionine and phenylalanine is respectively 20.94%, 19.06%, 38.12% and 12.00%, suggesting the potential of $Zn_{12}O_{12}$ nanocluster as a promising sensor for the detection of amino acids.

Useful information can be provided on the electronic properties of the obtained complexes through the analysis of frontier molecular orbitals isosurfaces. The frontier molecular orbitals of the studied complexes were generated with Multiwfn [65] and visualized with IboView program [66, 67]. As shown in Fig. 3, the HOMO's are almost entirely localized on the amino acids, whereas the LUMO's are predominantly localized on $Zn_{12}O_{12}$ nanocage with some contributions from the amino acids. Before the adsorption of the amino acids, the HOMO and LUMO energies of pristine $Zn_{12}O_{12}$ nanocluster were − 7.24 and − 2.99 eV, respectively. After their chemisorption, a quite significant changes were observed in HOMO and LUMO energies; the HOMO levels of PHE_$Zn_{12}O_{12}$, GLY_$Zn_{12}O_{12}$, TYR_$Zn_{12}O_{12}$ and MET_$Zn_{12}O_{12}$ complexes shift up to higher energies from -6.44 to -5.75 eV (− 6.44, − 6.41, − 6.31 and − 5.75 eV, respectively). The LUMO energies of TYR_$Zn_{12}O_{12}$ and PHE_$Zn_{12}O_{12}$ are shifted up (− 2.87 and − 2.70 eV) whereas those of GLY_$Zn_{12}O_{12}$ and MET_$Zn_{12}O_{12}$ are shifted down (− 3.05 and − 3.12 eV).

The orbital composition analysis shows that the HOMO of GLY_$Zn_{12}O_{12}$ comes mainly from the orbitals of nitrogen atom (64.8%), oxygen atoms (16.6%) and carbon atoms (12.6%); the HOMO of MET_$Zn_{12}O_{12}$ is localized mainly on the sulfur atom (86.4%), with a contribution of 8.8 and 4.6% from the hydrogen and carbon atoms, respectively. The HOMO of PHE_$Zn_{12}O_{12}$ is distributed on nitrogen atom (47.2%), oxygen atoms (30%) and carbon atoms (18%), while the HOMO of TYR_$Zn_{12}O_{12}$ complex is mainly composed of 41.8% (N), 30.2% (C) and 22.6% (O). The LUMO of all complexes is mainly localized on the Zn atoms of the $Zn_{12}O_{12}$ nanocluster.

Table 2 Thermodynamic parameters of the adsorption of amino acids on $Zn_{12}O_{12}$ nanocluster computed at B3LYP-D4/def2-TZVP in vacuum

Thermodynamic parameters	GLY_$Zn_{12}O_{12}$	TYR_$Zn_{12}O_{12}$	MET_$Zn_{12}O_{12}$	PHE_$Zn_{12}O_{12}$
ΔH° (kJ/mol)	− 156.08	− 213.92	− 158.78	− 201.89
ΔG° (kJ/mol)	− 102.84	− 148.06	− 100.92	− 133.59
ΔS° (kJ/mol)	− 53.26	− 65.90	− 57.91	− 68.32

Table 3 HOMO, LUMO, HOMO–LUMO gap (ΔEg) and HOMO–LUMO gap variation (ΔEg %) for $Zn_{12}O_{12}$, GLY_$Zn_{12}O_{12}$, TYR_$Zn_{12}O_{12}$, MET_$Zn_{12}O_{12}$ and PHE_$Zn_{12}O_{12}$ complexes

Electronic Parameters	$Zn_{12}O_{12}$	GLY_$Zn_{12}O_{12}$	TYR_$Zn_{12}O_{12}$	MET_$Zn_{12}O_{12}$	PHE_$Zn_{12}O_{12}$
E_{HOMO} (eV)	− 7.24	− 6.41	− 6.31	− 5.75	− 6.44
E_{LUMO} (eV)	− 2.99	− 3.05	− 2.87	− 3.12	− 2.70
$\lvert\Delta E_g\rvert$ (eV)	4.25	3.36	3.44	2.63	3.74
ΔE_g %	–	20.94	19.06	38.12	12.00

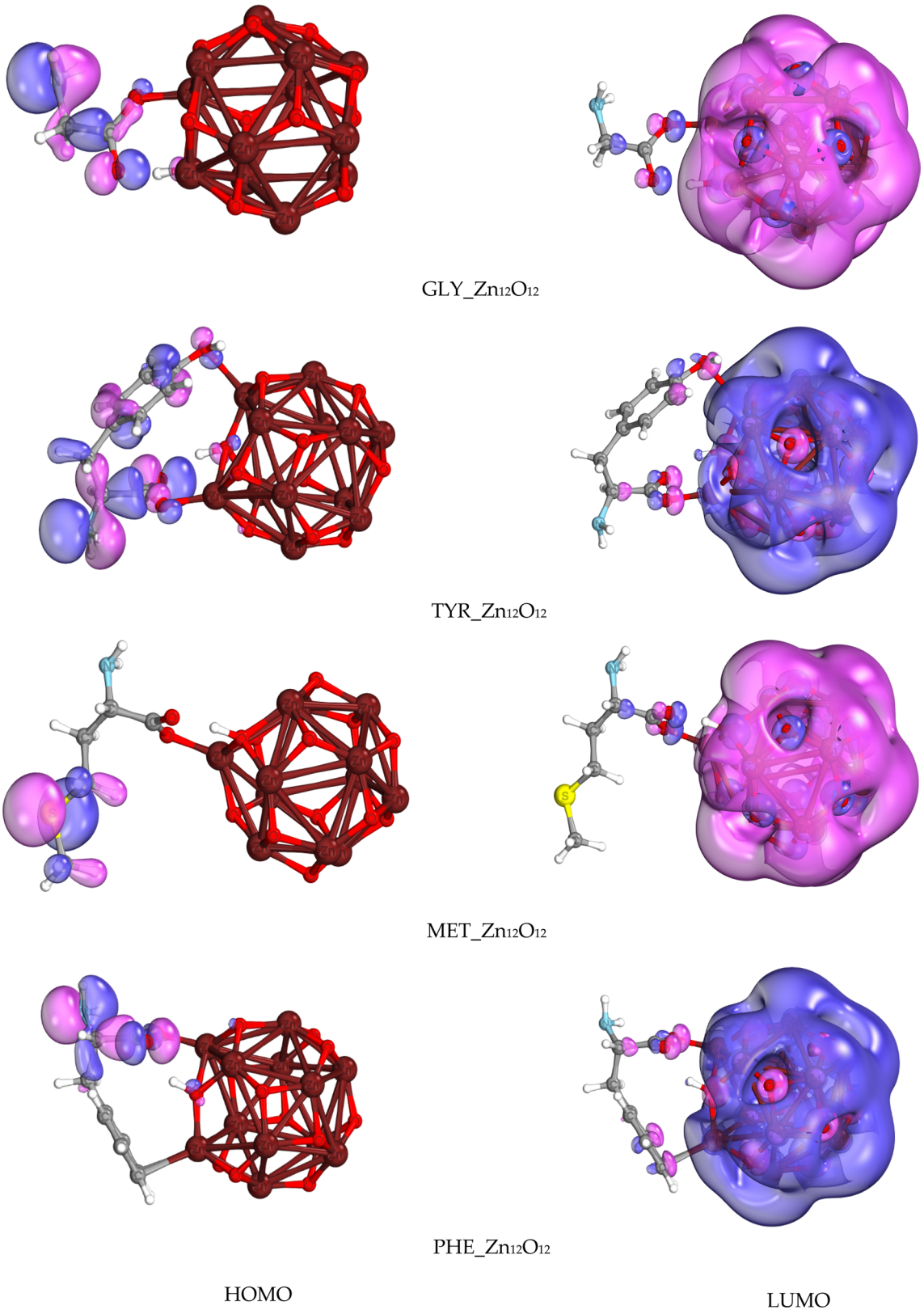

Fig. 3 Frontier molecular orbital isosurfaces for GLY_$Zn_{12}O_{12}$, MET_$Zn_{12}O_{12}$, TYR_$Zn_{12}O_{12}$ and PHE_$Zn_{12}O_{12}$ complexes

3.5 Charge transfer analysis

Multiwfn program was utilized to quantify the charge transfer based on the Mulliken method through the charge decomposition analysis (CDA) [65, 68] and its extended version (ECDA) [69]. ECDA analysis provides theoretical insight into the charge transfer process between two fragments, which can be characterized in the framework of ECDA approach by excluding the electronic polarization (PL). The CDA and ECDA results of the studied complexes are reported in Table 4. According to the CDA results, the number of donated electrons from $Zn_{12}O_{12}$ to the amino acids is in the range [0.236–0.305] a.u., while electrons back-donated from amino acids to $Zn_{12}O_{12}$ range from 0.226 to 0.396 a.u., indicating that both donation and back-donation are significantly involved in the electron transfer process. ECDA analysis shows that the net electrons obtained by glycine and methionine from $Zn_{12}O_{12}$ are 0.046 a.u. For TYR_$Zn_{12}O_{12}$ and PHE_$Zn_{12}O_{12}$ complexes, the net number of electrons obtained by $Zn_{12}O_{12}$ from tyrosine and phenylalanine is, respectively, 0.030 and 0.111.

3.6 Interaction region indicator (IRI) analysis

The optimized structures at B3LYP-D4/def2-TZVP-gCP level of theory were subjected to the interaction region indicator (IRI) analysis [70, 71] to explore the nature of the interaction regions occurring in each complex. The IRI approach is based on the charge density and its gradient to determine the intra- and intermolecular interactions in molecular systems in which both chemical bonding and weak interactions regions can be investigated. The IRI function is formulated as:

$$\mathbf{IRI}(\mathbf{r}) = \frac{|\nabla \boldsymbol{\rho}(\boldsymbol{r})|}{[\boldsymbol{\rho}(\boldsymbol{r})]^{a}}$$

where a parameter is set to the recommended value of 1.1 [71]. According to the values of sign of $\left(\lambda_2\right)\boldsymbol{\rho}$, the color mapping of IRI isosurfaces can reveal the nature of the interaction regions of interest. The isosurfaces are filled with the blue, green and red (BGR) color model, which correspond, respectively, to notable attractive forces, weak attractive interactions, and a notable repulsion. The covalent bonding regions are depicted by the blue circular disc-shaped isosurfaces. Figure 4 shows the IRI isosurfaces of GLY_$Zn_{12}O_{12}$, TYR_$Zn_{12}O_{12}$, MET_$Zn_{12}O_{12}$ and PHE_$Zn_{12}O_{12}$ complexes.

The IRI generated isosurfaces with an isovalue of 1.0 a.u confirm the presence of hydrogen bonds represented by the blue disc-shaped surfaces between O–H groups of the aminoacids and oxygen atoms of $Zn_{12}O_{12}$ nanocluster. The red spots observed in $Zn_{12}O_{12}$ and inside the aromatic rings of TYR_$Zn_{12}O_{12}$ and PHE_$Zn_{12}O_{12}$ complexes indicate a steric repulsion. The chemical bond regions in glycine, tyrosine, methionine and phenylalanine are revealed by the blue dumbbell-shaped discs as shown in Fig. 4. The green areas are attributed to the van der Waals interactions that are more significant for TYR_$Zn_{12}O_{12}$ and PHE_$Zn_{12}O_{12}$ than for GLY_$Zn_{12}O_{12}$ and MET_$Zn_{12}O_{12}$ complexes. It is important to point out that TYR_$Zn_{12}O_{12}$ and PHE_$Zn_{12}O_{12}$ complexes are associated with the highest complexation energies, suggesting that van der Waals interactions account for the stabilization of the formed complexes, and therefore, play a key role in the complexation process.

3.7 Molecular electrostatic potential

The molecular electrostatic potential, often known as MEP, is an extremely useful tool for the investigation of electron density clouds as well as the prediction of electrostatic effects and hydrogen bonding in molecular systems. These effects can be seen in nucleophilic or electrophilic regions. The molecular electrostatic potential maps calculated in vacuum at B3LYP-D4/def2-TZVP-gCP level of theory for GLY_$Zn_{12}O_{12}$, TYR_$Zn_{12}O_{12}$, MET_$Zn_{12}O_{12}$ and PHE_$Zn_{12}O_{12}$ complexes are plotted in Fig. 5 with Jmol program [72]. Coloring scheme is used to represent different levels of electron density in the range [-0.1, + 0.1 a.u.]: red color corresponds to high electron density (negative potential),

Table 4 Computed terms of donation (d), back-donation (b), (d-b), repulsive polarization (r) and the net electrons transferred from CDA and ECDA analysis

CDA analysis					ECDA analysis
Complex	d	b	d-b	r	Net electrons obtained by amino acid
GLY_$Zn_{12}O_{12}$	0.236	0.235	0.001	−0.283	0.046
MET_$Zn_{12}O_{12}$	0.236	0.226	0.010	−0.306	0.046
					Net electrons obtained by $Zn_{12}O_{12}$
TYR_$Zn_{12}O_{12}$	0.305	0.380	−0.075	−0.359	0.030
PHE_$Zn_{12}O_{12}$	0.241	0.396	−0.155	−0.307	0.111

d: the number of electrons donated from $Zn_{12}O_{12}$ to amino acid

b: the number of electrons back-donated from amino acid to $Zn_{12}O_{12}$

r: the number of electrons involved in repulsive polarization

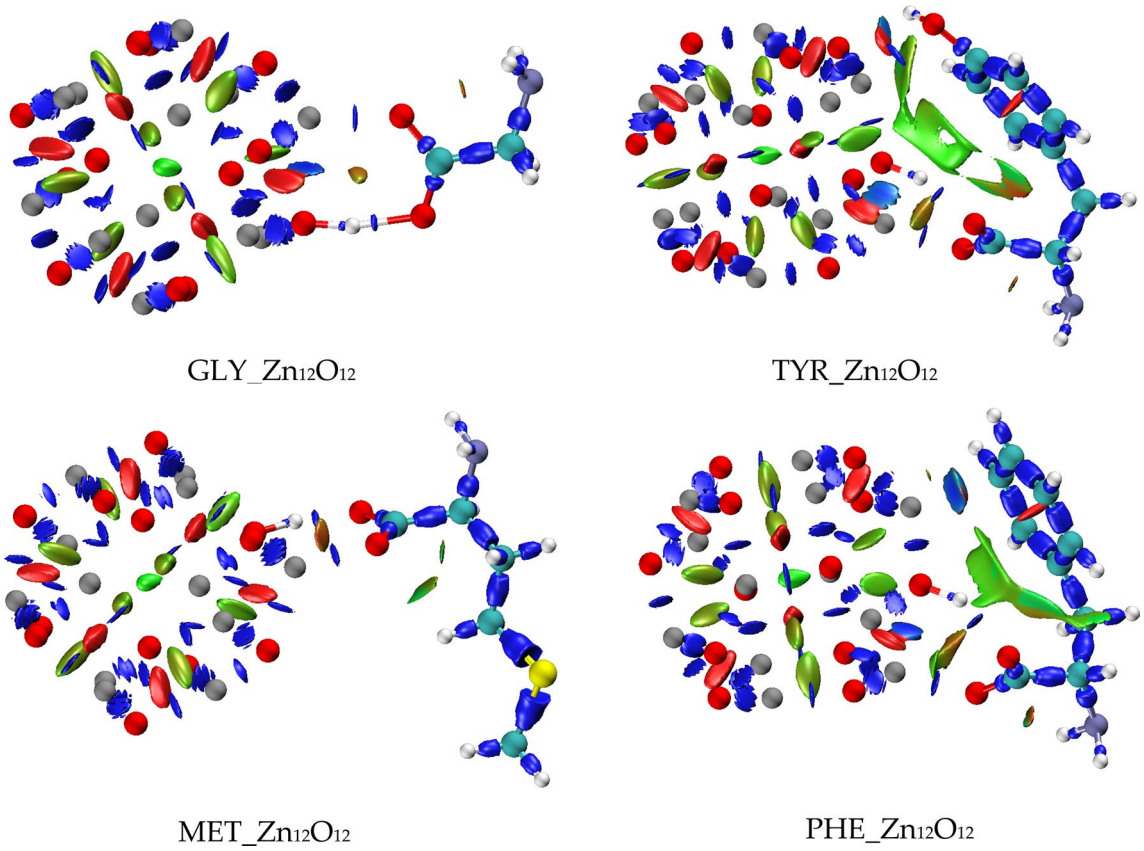

Fig. 4 Interaction region indicator isosurfaces (isovalue 1.0 a.u) for GLY_$Zn_{12}O_{12}$, MET_$Zn_{12}O_{12}$, TYR_$Zn_{12}O_{12}$ and PHE_$Zn_{12}O_{12}$ complexes

blue indicates low electron density (positive potential) and yellow and green represent respectively, moderate and neutral potentials.

Figure 5 reveals that the majority of the electron density is localized on the negatively charged oxygen atoms, which are indicated by the red color and represent the regions of most negative electrostatic potential. On the other hand, the regions of most positive electrostatic potential are localized on the positively charged zinc atoms of the $Zn_{12}O_{12}$ nanocluster, which are depicted by the blue color.

4 Conclusions

The current work investigated the interaction of ZnO nanocluster with the amino acids glycine, tyrosine, methionine and phenylalanine using the DFT-D4 approach. We were able to characterize the nature of the happening interactions by analyzing the structural, energetic and electronic features utilizing the thermodynamic parameters, the analysis of frontier molecular orbitals isosurfaces, and the charge decomposition analysis (CDA). Results indicated that the four amino acids interact with $(ZnO)_{12}$ via a chemisorption process, with adsorption energy values equal to − 147.83, − 207.50, − 161.72 and − 193.51 kJ/mol for GLY_$Zn_{12}O_{12}$, TYR_$Zn_{12}O_{12}$, MET_$Zn_{12}O_{12}$ and PHE_$Zn_{12}O_{12}$ complexes, respectively. Therefore, the interaction between the tyrosine and the $(ZnO)_{12}$ is the most favorable among the studied amino acids. The thermodynamic parameters such as the changes of Gibbs energy, enthalpy and entropy showed that the complexation is an exothermic process and driven by changes in enthalpy. The four complexes have a lower ΔEg (HOMO–LUMO gap) than isolated $Zn_{12}O_{12}$ and follow the decreasing order: PHE_$Zn_{12}O_{12}$ > TYR_$Zn_{12}O_{12}$ > GLY_$Zn_{12}O_{12}$ > MET_$Zn_{12}O_{12}$. The charge decomposition analysis results show that donation and back-donation are important in the electronic charge transfer. The results show also that hydrogen bonding and van der Waals interactions contribute to the complexation process, with the latter being more important for TYR_$Zn_{12}O_{12}$ and PHE_$Zn_{12}O_{12}$ complexes, therefore, ZnO nanoparticles can be considered as attractive nanobiosensors for amino acids and in particular for aromatic amino acids. These findings can be used as a guide to support the experimental works in the field of sensing applications.

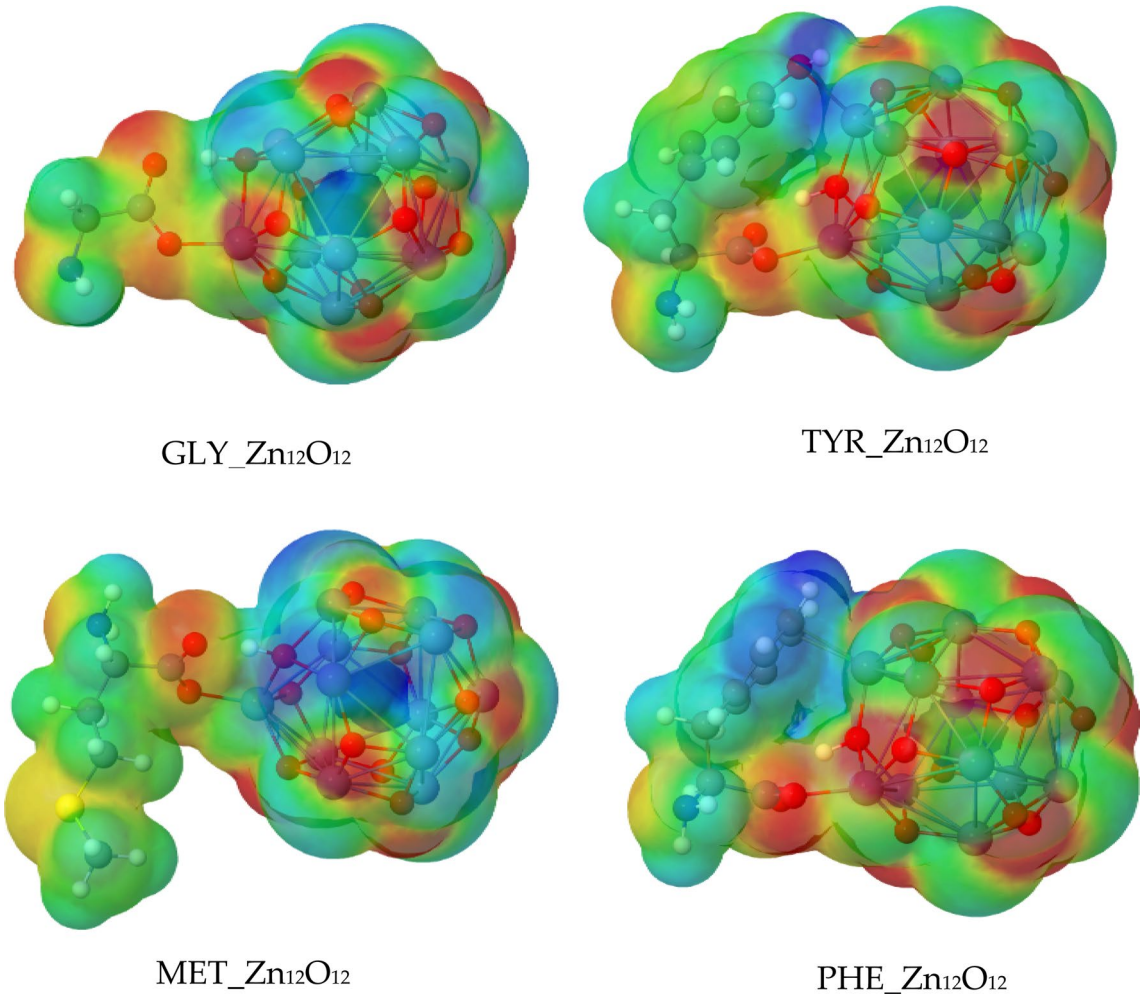

Fig. 5 Molecular electrostatic potential maps of GLY_$Zn_{12}O_{12}$, TYR_$Zn_{12}O_{12}$, MET_$Zn_{12}O_{12}$ and PHE_$Zn_{12}O_{12}$ complexes plotted using Jmol program

Author contributions SR, YB, MS contributed to conceptualization and methodology; MD, YB, MD done software; SR, YB, NS, MS done validation;, SR, MD, YB performed formal analysis; SR, MD, MD done investigation; YB and MS helped in resources; SR and YB helped in data curation; SR, MD, YB, NS, MD, MS helped in writ-ing—original draft preparation; SR, MD, YB, NS, MD, MS helped in writing—review and editing; SR done visualization; YB contributed to supervision. All authors have read and agreed to the published version of the manuscript.

Funding This research received no external funding.

Declarations

Conflicts of interest The authors declare no conflict of interest.

References

1. Pandya A, Shukla RK (2018) New perspective of nanotechnology: role in preventive forensic. Egypt J Forensic Sci 8(1):1–11
2. Bhatt PV, Pandey G, Tharmavaram M, Rawtani D, Mustansar HC (2020) Nanotechnology and Taggant Technology in Forensic Science. Technol Foren Sci Sampl Anal Data and Regulations 14:279–301
3. Bhatia T (2022) Novel nanomaterials in forensic investigations: a review. Mater Today: Proceedings 50:1071–1079
4. Bayford R, Rademacher T, Roitt I, Wang SX (2017) Emerging applications of nanotechnology for diagnosis and therapy of disease: a review. Physiol Meas 38(8):R183
5. Hassan DSM (2022) New perspective of calcium oxide nanoparticles in forensic science. Int J Electron Crime Invest 6(2):16–16
6. Peyghan AA, Baei MT, Hashemian S (2013) ZnO nanocluster as a potential catalyst for dissociation of H2S molecule. J Cluster Sci 24(1):341–347
7. Feng T, Chen Y, Hui D, Sun Z (2010) The patterned electron field emission of printed carbon nanotube films by image transfer technology. Vacuum 85(4):527–530

8. Wang Q, Zhang C, Shen G, Liu H, Fu H, Cui D (2014) Fluorescent carbon dots as an efficient siRNA nanocarrier for its interference therapy in gastric cancer cells. J Nanobiotechnol 12(1):1–12
9. Liang Z, Li X, Xie Y, Liu S (2014) 'Smart'gold nanoshells for combined cancer chemotherapy and hyperthermia. Biomed Mater 9(2):025012
10. Paul DR, Robeson LM (2008) Polymer nanotechnology: nanocomposites. Polymer 49(15):3187–3204
11. Senthilkumar K, Senthilkumar O, Yamauchi K, Sato M, Morito S, Ohba T, Morihiko N, Fujita Y (2009) Preparation of ZnO nanoparticles for bio-imaging applications. Physica status solidi (b) 246(4):885–888
12. Kotcherlakota R, Nimushakavi S, Roy A, Yadavalli HC, Mukherjee S, Haque S, Patra CR (2019) Biosynthesized gold nanoparticles: In vivo study of near-infrared fluorescence (NIR)-based bio-imaging and cell labeling applications. ACS Biomater Sci Eng 5(10):5439–5452
13. Pallares RM, Thanh NTK, Su X (2019) Sensing of circulating cancer biomarkers with metal nanoparticles. Nanoscale 11(46):22152–22171
14. Zhang Q, Jeppesen DK, Higginbotham JN, Graves-Deal R, Trinh VQ, Ramirez MA, Sohn Y, Neininger AC, Taneja N, McKinley ET, Niitsu H (2021) Supermeres are functional extracellular nanoparticles replete with disease biomarkers and therapeutic targets. Nat Cell Biol 23(12):1240–1254
15. George JM, Antony A, Mathew B (2018) Metal oxide nanoparticles in electrochemical sensing and biosensing: a review. Microchim Acta 185(7):1–26
16. Loiseau A, Asila V, Boitel-Aullen G, Lam M, Salmain M, Boujday S (2019) Silver-based plasmonic nanoparticles for and their use in biosensing. Biosensors 9(2):78
17. Litim A, Belhocine Y, Benlecheb T, Ghoniem MG, Kabouche Z, Ali FAM, Abdulkhair BY, Seydou M, Rahali S (2021) DFT-D4 Insight into the Inclusion of Amphetamine and Methamphetamine in Cucurbit [7] uril: Energetic, Structural and Biosensing Properties. Molecules 26(24):7479
18. Mitchell MJ, Billingsley MM, Haley RM, Wechsler ME, Peppas NA, Langer R (2021) Engineering precision nanoparticles for drug delivery. Nat Rev Drug Discovery 20(2):101–124
19. Haley B, Frenkel E (2008) Nanoparticles for drug delivery in cancer treatment. in Urologic Oncology: Seminars and original investigations. Elsevier
20. Suo X, Zhang J, Zhang Y, Liang XJ, Zhang J, Liu D (2020) A nano-based thermotherapy for cancer stem cell-targeted therapy. J Mater Chem B 8(18):3985–4001
21. Hamlaoui M, Hamlaoui I, Damous M, Belhocine Y, Sbei N, Ali FAM, Alghamdi MA, Taleb S, Rahali S, Merazig H (2022) Synthesis of two novel copper (II) complexes as potential inhibitors of HIV-1 protease enzyme: experimental and theoretical investigations. Crystals 12(8):1066
22. Fan Z, Lu JG (2005) Zinc oxide nanostructures: synthesis and properties. J Nanosci Nanotechnol 5(10):1561–1573
23. Zhang Y, Nayak RT, Hong H, Cai W (2013) Biomedical applications of zinc oxide nanomaterials. Curr Mol Med 13(10):1633–1645
24. Schwaminger S, Blank-Shim SA, Borkowska PM, Anand P, Fraga-García P, Fink K, Wenzel W, Berensmeier S (2018) Experimental characterization and simulation of amino acid and peptide interactions with inorganic materials. Eng Life Sci 18(2):84–100
25. Bazrafshan AA, Ghaedi M, Hajati S, Naghiha R, Asfaram A (2017) Synthesis of ZnO-nanorod-based materials for antibacterial, antifungal activities, DNA cleavage and efficient ultrasound-assisted dyes adsorption. Ecotoxicol Environ Saf 142:330–337
26. Bisht G, Rayamajhi S (2016) ZnO nanoparticles: a promising anticancer agent. Nanobiomedicine 3:3–9
27. Mukhlif BA, Patra I, Kumar TCA, Sivaraman R, Saadoon N, Obaid NH, Kumar NB, Mustafa YF (2022) Investigate the effect of Zn12O12, AlZn11O12, and GaZn11O12 nanoclusters in the carbamazepine drug detection in gas and solvent phases: a comparative DFT study. Monatshefte für Chemie-Chemical Monthly 154:171–179
28. Ma H, Hou Y, Fang H, Sarkar A (2021) Investigation of the interaction of amphetamine drug with Zn12O12 nanocage: a quantum chemical study. J Comput Electron 20(3):1065–1071
29. Zhihong Y, Ye Y, Pejhan A, Nasr AH, Nourbakhsh N, Tayebee R (2020) A theoretical study on the pure and doped ZnO nanoclusters as effective nanobiosensors for 5-fluorouracil anticancer drug adsorption. Appl Organomet Chem 34(4):e5534
30. Molina R, Al-Salama Y, Jurkschat K, Dobson PJ, Thompson IP (2011) Potential environmental influence of amino acids on the behavior of ZnO nanoparticles. Chemosphere 83(4):545–551
31. Nawrocki G, Cieplak M (2013) Amino acids and proteins at ZnO–water interfaces in molecular dynamics simulations. Phys Chem Chem Phys 15(32):13628–13636
32. Godymchuk A, Papina I, Karepina E, Kuznetsov D (2020) Behavior of ZnO nanoparticles in glycine solution: pH and size effect on aggregation and adsorption. Colloid Interface Sci Commun 39:100318
33. Chakraborty A, Boer JC, Selomulya C, Plebanski M (2017) Amino acid functionalized inorganic nanoparticles as cutting-edge therapeutic and diagnostic agents. Bioconjug Chem 29(3):657–671
34. Biswas S, Medina SH, Barchi JJ Jr (2015) Synthesis and cell-selective antitumor properties of amino acid conjugated tumor-associated carbohydrate antigen-coated gold nanoparticles. Carbohyd Res 405:93–101
35. Ghosh PS, Kim CK, Han G, Forbes NS, Rotello VM (2008) Efficient gene delivery vectors by tuning the surface charge density of amino acid-functionalized gold nanoparticles. ACS Nano 2(11):2213–2218
36. Lalatsa A, Schätzlein AG, Mazza M, Le TBH, Uchegbu IF (2012) Amphiphilic poly (l-amino acids)—new materials for drug delivery. J Control Release 161(2):523–536
37. Hall JC (1998) Glycine. J Parenter Enter Nutr 22(6):393–398
38. Hennig C, Takao S, Takao K, Weiss S, Kraus W, Emmerling F, Scheinost AC (2012) Structure and stability range of a hexanuclear Th (IV)–glycine complex. Dalton Trans 41(41):12818–12823
39. Chaudhuri P, Lima CN, Frota HO, Ghosh A (2021) Density functional study of glycine adsorption on single-walled BN nanotubes. Appl Surf Sci 536:147686
40. Irrera S, Costa D, Marcus P (2009) DFT periodic study of adsorption of glycine on the (0 0 0 1) surface of zinc terminated ZnO. J Mol Struct (Thoechem) 903:49–58
41. Dervin S, Ganguly P, Dahiya RS (2021) Disposable electrochemical sensor using graphene oxide–chitosan modified carbon-based electrodes for the detection of tyrosine. IEEE Sens J 21(23):26226–26233
42. Riemann A, Owens BE (2010) Molecular mechanics modeling of the adsorption of methionine on graphite. Surf Sci 604(23–24):2084–2090
43. Majd MM, Farrokhpour H, Chermahini AN, Dabbagh HA (2021) A comparative theoretical study of the chiral discrimination of phenylalanine enantiomers by the cyclic peptides with different sizes as discriminating agents: A DFT study. J Mol Struct 1243:130904
44. Messiad FA, Ammouchi N, Belhocine Y, Alhussain H, Ghoniem MG, Said RB, Ali FAM, Rahali S (2022) In search of preferential macrocyclic hosts for sulfur mustard sensing and recognition: a computational investigation through the new composite method r2SCAN-3c of the key factors influencing the host-guest interactions. Nanomaterials 12(15):2517

45. Rahali S, Belhocine Y, Allal H, Bouhadiba A, Assaba IM, Seydou M (2022) A DFT investigation of the host–guest interactions between boron-based aromatic systems and β-cyclodextrin. Struct Chem 33(1):195–206
46. Belhocine Y, Bouhadiba A, Rahim M, Nouar L, Djilani I, Khatmi DI (2018) Inclusion complex formation of β-cyclodextrin with the nonsteroidal anti-inflammatory drug flufenamic acid: computational study. Macroheterocycles 11(2):203–209
47. Kabouche Z, Belhocine Y, Benlecheb T, Assaba IM, Litim A, Lalalou R, Mechhoud A (2023) A DFT-D4 investigation of the complexation phenomenon between pentachlorophenol and β-cyclodextrin. Chimica Techno Acta 10(2):202310209
48. Belhocine Y, Rahali S, Allal H, Assaba IM, Ghoniem MG, Ali FAM (2021) A dispersion corrected DFT investigation of the inclusion complexation of dexamethasone with β-cyclodextrin and molecular docking study of its potential activity against COVID-19. Molecules 26(24):7622
49. Assaba IM, Rahali S, Belhocine Y, Allal H (2021) Inclusion complexation of chloroquine with α and β-cyclodextrin: theoretical insights from the new B97–3c composite method. J Mol Struct 1227:129696
50. Zhang S, Zhang Y, Huang S, Liu H, Wang P, Tian H (2011) Theoretical investigation of growth, stability, and electronic properties of beaded ZnO nanoclusters. J Mater Chem 21(42):16905–16910
51. Neese F (2012) The ORCA program system. Wiley Interdisciplinary Reviews: Computational Molecular Science 2(1):73–78
52. Neese F (2017) Software update: the ORCA program system, version 4.0. Wiley Interdiscip Rev-Comput Mol Sci 8(1):73–78
53. Neese F, Wennmohs F, Becker U, Riplinger C (2020) The ORCA quantum chemistry program package. J Chem Phys 152(22):224108
54. Becke AD (1988) Density-functional exchange-energy approximation with correct asymptotic behavior. Phys Rev A 38(6):3098
55. Lee C, Yang W, Parr RG (1988) Development of the Colle-Salvetti correlation-energy formula into a functional of the electron density. Phys Rev B 37(2):785
56. Weigend F, Ahlrichs R (2005) Balanced basis sets of split valence, triple zeta valence and quadruple zeta valence quality for H to Rn: design and assessment of accuracy. Phys Chem Chem Phys 7(18):3297–3305
57. Caldeweyher E, Bannwarth C, Grimme S (2017) Extension of the D3 dispersion coefficient model. J Chem Phys 147(3):034112
58. Neese F, Wennmohs F, Hansen A, Becker U (2009) Efficient, approximate and parallel Hartree-Fock and hybrid DFT calculations. A 'chain-of-spheres' algorithm for the Hartree-Fock exchange. Chem Phys 356(1–3):98–109
59. Goerigk L, Kruse H, Grimme S (2011) Benchmarking density functional methods against the S66 and S66x8 datasets for non-covalent interactions. ChemPhysChem 12(17):3421–3433
60. Chen Q, Wang J (2009) Structural, electronic, and magnetic properties of TMZn11O12 and TM2Zn10O12 clusters (TM= Sc, Ti, V, Cr, Mn, Fe Co, Ni, and Cu). Chem Phys Lett 474(4–6):336–341
61. Maddahi PS, Yeganeh M, Baghsiyahi FB (2019) ZnO nanoparticles as a sensitive platform for detection of nitration in tyrosine and tryptophan: A DFT study. Mater Chem Phys 237:121857
62. Roy Dennington TK, Millam J (2009) Gaussview, version 5. Semichem Inc., Shawnee Mission, KS
63. Tayebee R, Hosseini-Nasr A, Zamand N, Maleki B (2015) Density functional study on the adsorption of some aliphatic aldehydes on $(ZnO)_{12}$ and M-doped $(ZnO)_{12}$ nanocages. Polyhedron 102:503–513
64. Poor Heravi MR, Torkpour I, Vessally E, Amini I (2021) Adsorption of syn− propanethial S− oxide on the $Zn_{12}O_{12}$ cluster: insights from ab-initio modelling. J Sulfur Chem 42(3):308–321
65. Dapprich S, Frenking G (1995) Investigation of donor-acceptor interactions: a charge decomposition analysis using fragment molecular orbitals. J Phys Chem 99(23):9352–9362
66. Knizia G (2013) Intrinsic atomic orbitals: An unbiased bridge between quantum theory and chemical concepts. J Chem Theory Comput 9:4834–4843
67. Knizia G, Klein JE (2015) Electron flow in reaction mechanisms—Revealed from first principles. Angew Chem Int Ed 54:5518–5522
68. Meng X, Tian L (2015) Generalized charge decomposition analysis (GCDA) method. J Adv Phys Chem 4:111
69. Gorelsky SI, Ghosh S, Solomon EI (2006) Mechanism of N2O reduction by the μ4-S tetranuclear CuZ cluster of nitrous oxide reductase. J Am Chem Soc 128(1):278–290
70. Lu T, Chen Q (2023) Visualization analysis of weak interactions in chemical systems. Refer Mod Chem Mol Sci Chem Eng. https://doi.org/10.1016/B978-0-12-821978-2.00076-3
71. Lu T, Chen Q (2021) Interaction region indicator: a simple real space function clearly revealing both chemical bonds and weak interactions. Chemistry-Methods 1:231–239
72. Jmol: An Open-Source Java Viewer for Chemical Structures in 3D. Available online: http://www.jmol.org/ (accessed on 27 July 2023).